Video Article

Fracture Apparatus Design and Protocol Optimization for Closed-stabilized Fractures in Rodents

Robert L Zondervan[1,2], Mitch Vorce[3], Nick Servadio[4], Kurt D. Hankenson[2]

[1]College of Osteopathic Medicine, Michigan State University

[2]Department of Orthopaedic Surgery, University of Michigan Medical School

[3]Lymann Briggs College, Michigan State University

[4]College of Engineering, Michigan State University

Correspondence to: Kurt D. Hankenson at kdhank@umich.edu

URL: https://www.jove.com/video/58186
DOI: doi:10.3791/58186

Keywords: Medicine, Issue 138, Fracture, bone, model, femur, tibia, stabilized, murine, mice, rodent, protocol, optimization, guillotine

Date Published: 8/14/2018

Citation: Zondervan, R.L., Vorce, M., Servadio, N., Hankenson, K.D. Fracture Apparatus Design and Protocol Optimization for Closed-stabilized Fractures in Rodents. *J. Vis. Exp.* (138), e58186, doi:10.3791/58186 (2018).

Abstract

The reliable generation of consistent stabilized fractures in animal models is essential for understanding the biology of bone regeneration and developing therapeutics and devices. However, available injury models are plagued by inconsistency resulting in wasted animals and resources and imperfect data. To address this problem of fracture heterogeneity, the purpose of the method described herein is to optimize fracture generation parameters specific to each animal and yield a consistent fracture location and pattern. This protocol accounts for variations in bone size and morphology that may exist between mouse strains and can be adapted to generate consistent fractures in other species, such as rat. Additionally, a cost-effective, adjustable fracture apparatus is described. Compared to current stabilized fracture techniques, the optimization protocol and new fracture apparatus demonstrate increased consistency in stabilized fracture patterns and locations. Using optimized parameters specific to the sample type, the described protocol increases the precision of induced traumas, minimizing the fracture heterogeneity typically observed in closed-fracture generation procedures.

Video Link

The video component of this article can be found at https://www.jove.com/video/58186/

Introduction

Research on fracture healing is necessary to address a large clinical and economic problem. Each year over 12 million fractures are treated in the United States[1], costing $80 billion per year[2]. The likelihood of a male or female suffering a fracture in their lifetime is 25% and 44%, respectively[3]. Problems associated with fracture healing are expected to increase with increased comorbidities as the population ages. To study and address this problem, robust models of fracture generation and stabilization are required. Rodent models are ideally suited for this purpose. They provide clinical relevance and can be modified to address specific conditions (*i.e.*, multiple injuries, open, closed, ischemic, and infected fractures). In addition to replicating clinical scenarios, animal fracture models are important for understanding bone biology and developing therapeutics and devices. However, attempts to study differences between interventions may be complicated by the variability introduced by inconsistent fracture generation. Thus, generating reproducible and consistently closed fractures in animal models is essential to the field of musculoskeletal research.

Despite properly controlling for potential subject heterogeneity by ensuring the appropriate genetic background, sex, age, and environmental conditions, the production of clinically-relevant consistent bone injuries is a significant variable affecting reproducibility that must be controlled. Statistical comparisons using inconsistent fractures are plagued with experimental noise and a high variability[4]; in addition, fracture variability can result in unnecessary animal death because of the need to increase the sample size or the necessity to euthanize animals with comminuted or malpositioned fractures. The purpose of the method described herein is to optimize the fracture generation parameters that are specific to sample type and yield a consistent fracture location and pattern.

Current models of fracture generation fall into two broad categories, each with their own strengths and weaknesses. Open-fracture (osteotomy) models undergo surgery to expose the bone, after which a fracture is induced by cutting the bone or weakening it and then manually breaking it[5,6,7,8]. The benefits of this method are the direct visualization of the fracture site and a more consistent fracture location and pattern. However, the physiological and clinical relevance of the approach and mechanism of injury is limited. Additionally, open methods of fracture generation require a surgical approach and closure with prolonged periods during which the rodents are exposed to an increased risk of contamination.

Closed techniques address many of the open technique's limitations. Closed techniques produce fractures using an externally applied blunt force trauma which induces injury to the bone and surrounding tissues, more similar to those seen in human clinical injuries. The most common method was described by Bonnarens and Einhorn in 1984[9]. They described a weighted guillotine being used to impart blunt trauma to break the bone without causing any external skin wounds. This method has been widely adopted to study the effect of genetics[10,11], pharmacologic

therapy[12,13,14,15], mechanics[16,17], and physiology[18,19,20] on bone healing in mice and rats. While the benefit of closed methods is physiologically relevant fractures, experimental reproducibility and rigor are limited by fracture heterogeneity. The inconsistent fracture generation results in a limited between-group differentiation, lost specimens, and an increase in animals needed to achieve statistical significance.

Controlling the variability in fracture generation and stabilization is essential to produce meaningful results. In order to properly study the biology of fracture repair, a simple yet robust fracture model is needed. The model should be translatable to rodent species, bone types (femur or tibiae, for example), and across variable mouse genetic backgrounds and induced mutations. Furthermore, the ideal procedure should be technically simple and produce consistent results. To address fracture heterogeneity, the method described herein is the construction of a well-controlled fracture device that can then be used to optimize parameters and generate consistently closed fractures regardless of age, sex, or genotype.

Protocol

This protocol was developed to ensure that animals are not used needlessly and are spared all unnecessary pain and distress; it adheres to all applicable federal, state, local, and institutional laws and guidelines governing animal research. The protocol was developed under the guidance of a university-wide Laboratory Animal Medicine Program directed by veterinarians specialized in laboratory animal medicine. The protocol was reviewed and approved by the Institutional Animal Care and Use Committee (IACUC).

1. Fracture Tower Construction

Note: All parts are listed in the materials section (**Table of Materials**). Detailed technical drawings are provided for the machined and 3D-printed parts in **Supplementary Figures 1-12**. The subassembly technical drawings include fastener details for all mounted parts (**Supplementary Figures 1, 2, 7,** and **9**).

1. **Support subassembly**
   NOTE: For a technical drawing of the support subassembly, see **Supplementary Figure 1**.
   1. Attach the **Beam Support--Jaw Section** at the midpoint of the **Beam Support--Horizontal Section**.
   2. Attach the **Beam Support--Vertical 1** to the top surface of the **Beam Support--Jaw Section**, 2 in from the **Beam Support--Horizontal Section**.
   3. Attach the **Beam Support--Vertical 2** to the top surface of the **Beam Support--Horizontal Section** at the midpoint (7 in from the end).
   4. Attach the **Beam, Support--Plate Mount** to the end of both **Beam Support--Vertical 1** and **Beam Support--Vertical 2**. The end of the plate support should be flush with the back of **Beam Support--Vertical 2**.

2. **Ram subassembly**
   Note: For a technical drawing of the ram subassembly, see **Supplementary Figure 2**.
   1. Machine the **Block Stop** and the **Block Guide** (**Supplementary Figure 3**); the **Rod Ram** (**Supplementary Figure 4**); the **Screw Alignment** (**Supplementary Figure 5**); and the **Plate Mounting** (**Supplementary Figure 6**).
   2. Attach the **Plate Mounting** to the **Beam Support--Plate Mount** of the support subassembly.
   3. In the following order, slide the first **Linear Sleeve Bearing**; the **Block Guide**; the second **Linear Sleeve Bearing**; and the **Block Stop** on the **Rod Ram**. Attach the guides and the blocks to the **Plate Mounting**.
   4. Attach three ⅜-in nuts to the threaded portion of the **Rod Ram**. One should be flush with the end of the rod to engage with the electromagnet. The other 2 will be used to adjust the fracture depth.
   5. Align the grove in the **Rod Ram** to face forward and insert the **Alignment Screw** into the threaded hole of the **Block Guide**.

3. **Magnet subassembly**
   Note: For a technical drawing of the magnet subassembly, see **Supplementary Figure 7**.
   1. Solder the **Electromagnet** leads to the wire (polarity is not a factor for the electromagnet operation). Allow enough length to reach the floor, where the fracture device will be positioned. Use zip ties or another form of attachment to stress relieve the wire.
   2. Strip the **Power Supply**'s end and connect it to the **Foot Pedal**. Finally, connect the wire to the **Foot Pedal** in an "off" (normally open) configuration. Test the circuit to ensure the **Electromagnet** is on when the **Foot Switch** is not pressed. This will hold the ram up before the fracture.
   3. Print the **Mount Magnet** (**Supplementary Figures 8A** and **8B**) using an additive manufacturing device, or machine the part from aluminum.
   4. Attach the **Electromagnet** to the **Mount Magnet**.
   5. Attach 2 **Corner Brackets** to the **Beam Support--Magnet**.
   6. In the following order, thread the **Rod Magnet** through the top **Corner Bracket** and add one ¼-in nut; the **Mount Magnet**; two ¼-in nuts; and the bottom **Corner Bracket**. Secure the assembly with two ¼-in nuts on each end.

4. **Complete assembly**
   Note: For a technical drawing of the complete assembly, see **Supplementary Figure 9**.
   1. Attach the **Magnet Subassembly** to the top surface of the **Beam, Support--Plate Mount**.
   2. Adjust the alignment of the **Beam Support--Magnet** so the magnet engages with the **Rod, Ram**.
      NOTE: If the rod does not release when the foot pedal is pressed, reduce the contact area between the electromagnet and the rod by moving the **Beam Support--Magnet**.
   3. Machine the **Brackets Leg Jaw** (**Supplementary Figure 10**).
   4. Attach the two **Brackets Leg Jaw** to the **Beam Support--Jaw Section**. When dropped, the tip of the ram should be at an equal distance from each jaw.
   5. Place the **Platform Fracture** (**Supplementary Figures 11A** and **11B**) above the jaws.
   6. Print the **Jig Positioning Fracture** (**Supplementary Figures 12A** and **12B**) and the **Jig Pin Gauge** (**Supplementary Figures 13A** and **13B**) using an additive manufacturing device, or machine the parts from aluminum.

NOTE: The dimensions of the **Jigs** will be calculated in the optimization steps detailed in step 2.
7. Attach the **Jig Positioning Fracture** to the **Platform Fracture**.
8. Confirm that the depth of the impact can be adjusted using the two stop nuts on the **Rod Ram**.
9. Confirm that the speed of the impact can be adjusted by moving the **Mount Magnet** up and down.
10. Confirm that the width of the fracture can be adjusted by moving the **Brackets Leg Jaw** closer or further away from the **Rod Ram**.

2. Fracture Optimization

1. **Fracture location**
    1. Obtain radiographs of the limb (femur or tibia) to be fractured in a representative sample of 5 euthanized animals.
    NOTE: The sample should be matched to the specimens, which will be used in the experimental protocol based on age, genotype, and sex. Even if the final protocol calls for only one fractured limb, both sample limbs will be used.
    2. Position the limb tangential to the x-ray beam to acquire true-lateral and anterior/posterior views to the bone. Place an object of known dimension at the imaging plane to provide a scale for analysis.
    3. Note: If imaging femurs, ensure the limb is in full extension, where the femur is in the same axial plane as the tibia.
    4. Mark the desired location of the fracture on the radiograph of the limb to be fractured (**Figure 1A** - dashed line). Measure from the calcaneal-tibial joint to the level of the marked fracture (**Figure 1A**). Calculate the mean fracture length (*FL*) for all trial specimens. Measure from the intercondylar notch for femur fractures.

2. **Fracture-positioning jig**
    1. Measure the distance from the outside surface of one support anvil to the center of the guillotine impact (CGI) (**Figure 2**). Subtract the *CGI* from the *FL*, described in step 2.1.4, to calculate the fracture-positioning jig depth (*JD*). Machine or 3D-print a U-shaped channel with a height and a width equal to the anvil, and a depth equal to the *JD* (**Figure 3A**). A sample technical drawing and CAD file are included in **Supplementary Figures 12A** and **12B**.
    NOTE: When the limb is placed in the jig, the dorsum of the foot should lie against the surface furthest from the guillotine impact. Modify the U-shaped channel if additional clearance is required for the limb.
    2. Position the specimen in the fracture apparatus in the prone position for femur fractures or in the supine position for tibia fractures (**Figure 4**). Press the dorsum of the foot against the end of the fracture-positioning jig. Manually depress the guillotine until the limb fractures. Obtain a radiograph of the fractured limb to confirm the jig size and fracture location (**Figure 2B**).
    3. Increase *JD* if the fracture location is too distal on the bone, or decrease *JD* if the fracture location is too proximal on the bone.

3. **Stabilization of the pin parameters**
    1. **Pin length:** Using the radiographs obtained in step 2.1, measure the limb length (*LL*) from the tibial plateau to the level of the posterior malleolus for tibia fractures, or the intercondylar notch to the greater trochanter for femur fractures. Multiply the bone length by 0.9 to calculate the pin length (*PL*) (**Figures 1A** and **3B**).
    2. **Pin Width:** Using the radiographs obtained in step 2.1, measure the minimum medullary diameter (*MD*) in the fractured limb (**Figure 1A**). Select a needle with a gauge approximately equivalent to the medullary diameter and a length more than 1.5 x *PL*.
    NOTE: An approximate pin size for a 14-week-old C57BL/6J mouse is 22 G, 1½ in and 27 G, 1¼ in for femur and tibia, respectively.

4. **Pin cutting gauge**
    1. 2.4.1. Machine or 3D-print a gauge with a length equal to *PL* minus the needle length (*CGL*) (**Figure 3B**; **Supplementary Figures 13A** and **13B**). One end should have an overhang to rest against the hub of the needle and the other should indicate where the pin should be cut. A sample technical drawing and CAD file are included in **Supplementary Figures 13A** and **13B**.

5. **Intramedullary pin fracture stabilization**
    1. Using the non-fractured trial specimens from step 2.1, remove hair with an electric clipper or depilatory cream from mid-tibia to mid-femur, exposing the knee joint.
    2. **Tibia pinning**: Insert the needle percutaneously lateral to the patellar ligament. Retract the patellar ligament medially and align the tip of the needle to the axis of the tibia. Using a reaming motion, gently breach the tibial plateau and guide the needle down the medullary cavity.
    3. **Femur pinning**: Insert the needle percutaneously lateral to the patellar ligament. Retract the patellar ligament medially and align the tip of the needle to the axis of the femur in the intercondylar notch. Using a reaming motion, gently breach the articular surface of the intercondylar notch and guide the needle down the medullary cavity.
    4. Using the gauge manufactured in step 2.4, ream until the exposed needle is equal to the gauge length. Retract the needle to provide enough room (~3 mm) to cut the needle at the level indicated by the gauge.
    NOTE: Be sure to hold the proximal (plastic) end of the needle while cutting, so it does not become a hazardous projectile.
    5. Crimp 0.3 mm of the distal end of the pin using a pin cutter and then cut the pin at the level of the gauge. Sink the pin to the articular surface using a rod with a diameter 1.5x larger than the diameter of the needle.
    NOTE: Crimping prevents rotation of the needle and migration by increasing the needle-bone contact.
    6. Obtain radiographs to confirm the needle extends the length of the medullary canal of the limb and does not protrude from the proximal or distal end (**Figure 1C**).

6. **Impact depth**
    1. Using the radiographs obtained in step 2.1, measure the diameter of the cortex at the level of the desired fracture (**Figure 1A**). Calculate the mean cortical diameter (*CD*) for all trial specimens.
    2. Position a pinned trial specimen from step 2.5 in the fracture device with the fracture-positioning jig manufactured in step 2.2. Rest the impact ram on the uninjured limb.
    NOTE: Do not allow the ram to drop; the bone should remain intact during this optimization step.

3. Apply enough downward force on the ram to compress soft tissue, but not fracture the bone. Adjust the impact depth (*ID*) to 0.75 x *CD* (**Figure 2**).
   NOTE: The ideal impact depth is 0.5 x *CD* when fracturing a bone without any soft tissue. Using 0.75 accounts for the additional soft-tissue compression.

7. **Anvil width**
   1. Set the anvil width (*AW*) to 0.4 cm for the mouse tibia or femur (**Figure 2**).
      NOTE: A wider width is recommended for larger specimens such as rats.

8. **Ram weight**
   1. A minimum weight of 250 g is recommended for murine specimens.
      NOTE: Additional weight can be threaded on to the ram for larger specimens (**Figure 2**).

9. **Impact velocity**
   1. Set the drop height (*DH*) to 2 cm (**Figure 2**). Position the ram in its starting position by connecting it to the activated electromagnet.
   2. Position a trial limb in the fracture apparatus. Press the dorsum of the foot against the fracture-positioning jig manufactured in step 2.2. Briefly depress the footswitch to release the ram and then reset it to its starting position.
   3. Radiograph the impacted trial limb. Analyze the limb for any evidence of a fracture (**Figure 1D**).
      NOTE: This can be subtle when using low velocities with a controlled impact depth.
   4. If no fracture is generated, repeat steps 2.9.1 - 2.9.3 and increase the drop height by 2 cm.
   5. If a fracture is generated, record the drop height, and multiply it by 1.1. This is the new *DH*.
   6. Using the *DH* from step 2.9.5, fracture the next trial limb.
   7. If no fracture is generated, repeat steps 2.9.1 - 2.9.6 and increase the drop height by 2 cm.
   8. If a fracture is generated, repeat steps 2.9.6 - 2.9.7 until all test samples are used. Record the final *DH* and all parameters (*FL*, *CGI*, *JD*, *PL*, *MD*, *PS*, *CGL*, *CD*, *ID*, *AW*, and *RW*) from the optimization. Record the trial specimens' age, sex, genotype, and weight.

3. Closed-stabilized Fracture Generation

1. **Set-up**
   1. Sterilize all equipment and instruments *via* autoclave, hot bead immersion, or their equivalent.
   2. Place a heating element on the surgical table and set it to the optimal temperature. Cover the element with a surgical drape. Prepare 3 x 3 in^2 of surgical drape with a 0.75-in circle cut out in the middle.
   3. Confirm the adjustment of the fracture tower before each trial (**Figure 2**). Set the *ID*, *AW*, *RW*, and *DH* to the values derived from the optimization protocol specific to the sex, age, and genotype for the specimen to be studied.
   4. Weigh and record the weight of the animal.

2. **Surgery**
   1. Adequately sedate the mouse using inhalant anesthetics (isoflurane: 4 - 5% for induction; 1 - 2% for maintenance) or another established laboratory anesthesia protocol. The respiratory rate should be 55 - 100 breaths/min. The animal should not be responsive to a hind-limb toe pinch.
   2. Administer the first dose of the postoperative analgesia buprenorphine (0.1 mg/kg subcutaneously).
   3. Apply ocular lubrication to prevent corneal drying.
   4. Remove the animal's hair with an electric clipper from mid-tibia to mid-femur, exposing the knee joint. Clean the site of excess hair using non-reactive tape. Prepare the pinning site with a wet swab moistened with 70% EtOH. Repeat as necessary to remove all hair from the incision area.
   5. Prepare and clean the pinning area with alternative swabs of povidone-iodine and 70% EtOH. Use two alternative swab sequences to ensure sterility.
   6. A drape is then placed around the surgical site after the skin has been appropriately disinfected.
   7. Pin the limb to be fractured using the protocol described in step 2.5. Acquire radiographs to confirm the pin extends the length of the medullary canal but does not protrude from the proximal or distal end.
   8. Turn on the electromagnet and connect the impact ram to place it in the starting position.
   9. Position the specimen in the fracture apparatus by placing it in a prone position for femur fractures or in a supine position for tibia fractures. The pinned limb should be placed across the anvils and in the fracture-positioning jig with the dorsum of the foot pressed against the outside of the jig.
   10. While pressing the foot with one hand and ensuring only the limb is in the impact ram target area, briefly depress the footswitch to release the ram. Replace the ram in the starting position.
   11. Acquire radiographs and confirm the fracture location and type.

3. **Postoperative management**
   1. Monitor the animal every 15 min during its recovery from anesthesia until the animal is conscious, can maintain sternal recumbency, and is ambulatory. Confirm the animal is able to ambulate over a 72-h period.
   2. House the animal individually until it has completely recovered.
   3. Maintain analgesia over a 48-h period with buprenorphine (0.1 mg/kg subcutaneously) administered every 12 h.
   4. Monitor and record the health status of the animal daily for 7 - 10 d or until euthanasia.

4. **Post-fracture analysis**
   1. Measure *FL*, *PL*, *CD*, *MD,* and the fracture pattern. Record the measurements in a master data file.

Representative Results

The guillotine previously used in our laboratory was developed in 2004 and was based on models published by Einhorn[21]. The design did not permit adjustments to adequately account for any differences in bone morphology and did not permit a reproducible positioning of the limb. Furthermore, the previous apparatus required two people to operate it. Therefore, we designed, engineered, and built a new fracture apparatus. The main design goal was the possibility to the high-fidelity adjustment of the fracture depth, impact force, three-point contact, and animal positioning. The design is based on a fracture apparatus described by Marturano in 2008[22]. A limiting factor of their design was the link between the fracture depth and the impact speed. The impact speed could not be adjusted without changing the fracture depth and the animal positioning. This made it impossible to change just one variable at a time when optimizing the fracture parameters. Additionally, it did not provide a way to easily adjust the location of a fracture in a long bone. Modifying how the depth of the fracture and the ram speed is adjusted, the design presented here permits a high-resolution, independent adjustment of all fracture variables. Additionally, the apparatus can be operated by a single user, it is cost-effective, and it allows adjustable animal positioning for generating location-specific fractures.

An optimization of tibia fractures in 17-week-old C57BL/6J male mice was performed using five specimens. The goal was to generate simple transverse fractures just below the level of the insertion of the fibula into the tibia. The distal tibia site is a common site of human bone fracture that results in non-union and, additionally, provides a homogeneous region of the tibia and avoids complications in the analysis associated with fibula damage. Mice were euthanized and radiographed. The mean *FL* from the calcaneal-tibial joint to the distal portion of the insertion of the fibula into the tibia was 0.556 ± 0.025 cm. Using an anvil width of 0.4 cm, the CGI was 0.2 cm, from which a *JD* of 0.356 cm was calculated. A positioning jig was constructed using computer-aided design software and printed at a resolution of 0.01 mm in acrylonitrile butadiene styrene (ABS) using a 3D printer (**Figure 3B**). Using one trial tibia, the jig design and the location of the fracture was confirmed by radiograph (**Figure 1B**).

For the results presented herein, the *PL* was calculated to be 1.579 cm, based on 90% of the mean tibial length (1.754 ± 0.031 cm). The mean medullary diameter (*MD*) was 0.05 cm. A needle size of 27 G x 3.175 cm was selected to exceed the necessary *PL* and fill the intramedullary canal (27 G = 0.041 cm). A cutting gauge was constructed with a length of 1.596 cm to demarcate the level of pin cutting (**Figure 3B**). Each of the remaining nine tibiae was then pinned. The mean cortical diameter was 0.098 cm, which was used to calculate an impact depth (*ID*) of 0.073 cm.

The initial tibia was impacted at a drop height of 1 cm, which resulted in no fracture. The drop height was increased by 1 cm to 2 cm. The new height resulted in a simple transverse fracture. For the subsequent fracture, the drop height was increased by 10% to 2.2 cm. This produced a simple transverse fracture on the first drop. All the remaining tibia fractured at 2.2 cm. In total, 9/9 (100%) of the pinned and fractured tibia resulted in simple transverse fractures without pin bending. The percentage of the experimental pin length to the target pin length and the experimental fracture length to the target fracture length were 101.1% and 97.6%, respectively. The final parameters are reported in **Table 1**, which also includes representative femur data.

Using the optimized parameters developed above, a trial was undertaken to compare pre- and post-optimization fractures. Retrospective radiographs were obtained from previous tibia fractures that were generated in our lab using a simple guillotine[21] without optimization. Briefly, the tibiae were pinned using a 0.029-cm wire. The wire was inserted until resistance was felt, retracted 3 mm, cut, and driven into place. Subsequently, the mouse was placed under the guillotine with the point of impact approximately at the insertion of the fibula into the tibia. The guillotine was then dropped from a level of 10 cm. An additional dataset of fractures was collected which were generated using the adjustable guillotine and parameters derived from the optimization protocol (**Table 1**). Each group contained 58 fractures in 14-week-old, genotype-matched mice. The radiographs were analyzed for experimental fracture length (EFL): the distance from the calcaneal-tibial joint to the fracture, the experimental pin length (EPL), the bone length, and the fracture pattern.

Using an adjustable fracture device and optimized parameters significantly ($p < 0.001$) improved the generation of simple transverse fractures (**Figure 5**). The pre-optimization group only generated a simple transverse fracture 46.55% (27/58) of the time, compared to the post-optimization group which generated a simple transverse fracture 98.28% (57/58) of the time. Only one specimen in the post-optimization group had a complex fracture due to a malalignment in the positioning jig. Based on the methods described in the optimization protocol, the cut pin length should capture 90% of the total bone length. Using the optimization parameters and the pin cutting gauge, the percentage of the experimental pin length to bone length in the post-optimization group was 92.43% compared to only 83.67% in the pre-optimization group ($p < 0.001$). The optimization also significantly decreased the variability of the fracture locations, the pin length, and the pin-to-bone length percentage ($p < 0.001$). The results are reported in **Table 2**.

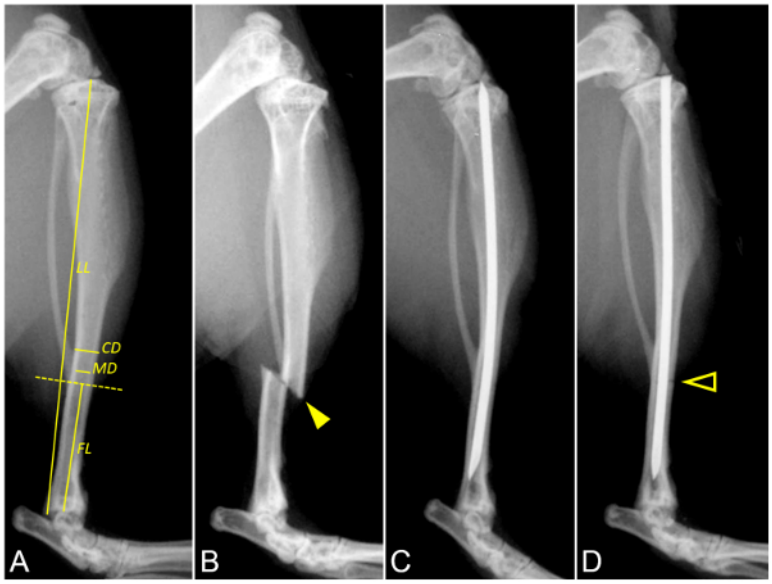

Figure 1: The optimization and generation of a simple tibia fracture. These panels show lateral radiographs of a murine tibia. (**A**) This panel shows the pre-fracture measurements. The dashed yellow line marks the ideal fracture location. The measurement overlays for the fracture length (*FL*), limb length (*LL*), medullary diameter (*MD*), and cortical diameter (*CD*) are indicated in the radiograph. (**B**) This panel shows a fracture location test. The solid arrowhead indicates the level of fracture in a non-stabilized tibia to test the positioning jig parameters. (**C**) This panel shows a pin length test with a pre-fracture radiograph to test the pin length (*PL*) and cutting gauge. *PL* should be 90% of *LL,* fill the intramedullary canal, and not protrude proximally or distally. (**D**) This panel shows a post-optimization fracture generation. The arrowhead outline indicates the level of the simple transverse tibia fracture. The pin is not bent at the level of impact. Please click here to view a larger version of this figure.

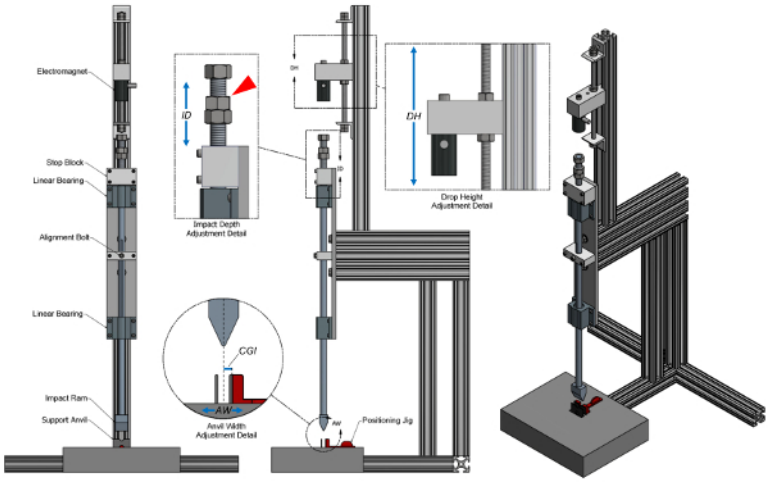

Figure 2: Adjustable fracture device design. This figure shows frontal, lateral, and perspective views of the fracture device. The frontal view includes annotations of major device components. The lateral view includes magnified details illustrating the adjustments for the impact depth (*ID*), the drop height (*DH*), and the anvil width (*AW*). Additional weight can be added to the ram by threading on weights at the top of the impact ram indicated by the red arrowhead. The dotted line in the Anvil Width Adjustment Detail indicates the line of impact. The center of guillotine impact to the outside surface a support anvil (*CGI*) is used to calculate the depth of the positioning jig to produce an accurate and precise fracture level. The positioning jig is shown in detail in **Figure 3A**. Please click here to view a larger version of this figure.

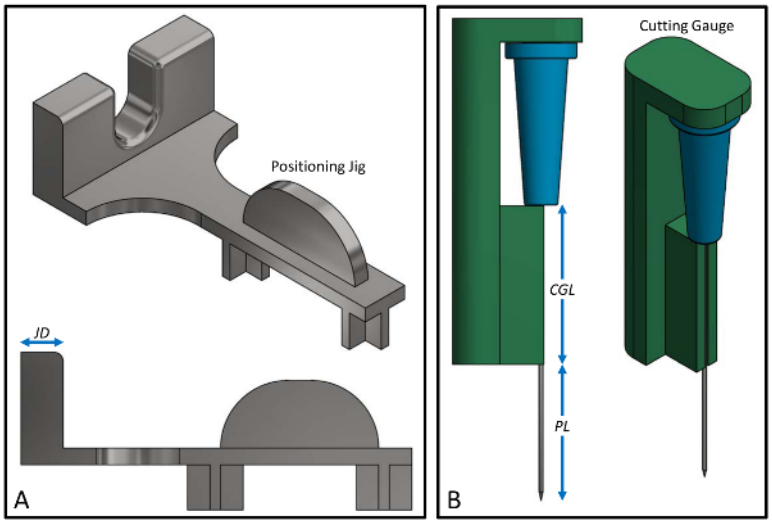

Figure 3: Positioning jig and cutting gauge design. (**A**) This panel shows details of the mouse positioning jig. The jig depth (*JD*) can be adjusted to change the fracture location on the limb. Increasing *JD* will move the fracture proximally and decreasing *JD* will move the fracture distally. (**B**) This panel shows details of the needle and the pin cutting gauge. The pin length (*PL*) should be 90% of the limb length (*LL*) (**Figure 1A**). The cutting gauge length (*CGL*) is derived from subtracting the *PL* from the needle length. In this example, a cutting gauge has been constructed (*CGL* = 1.6 cm) to demarcate a 27-G needle (length = 3.175 cm), leaving a *PL* of 1.58 cm after cutting. Please click here to view a larger version of this figure.

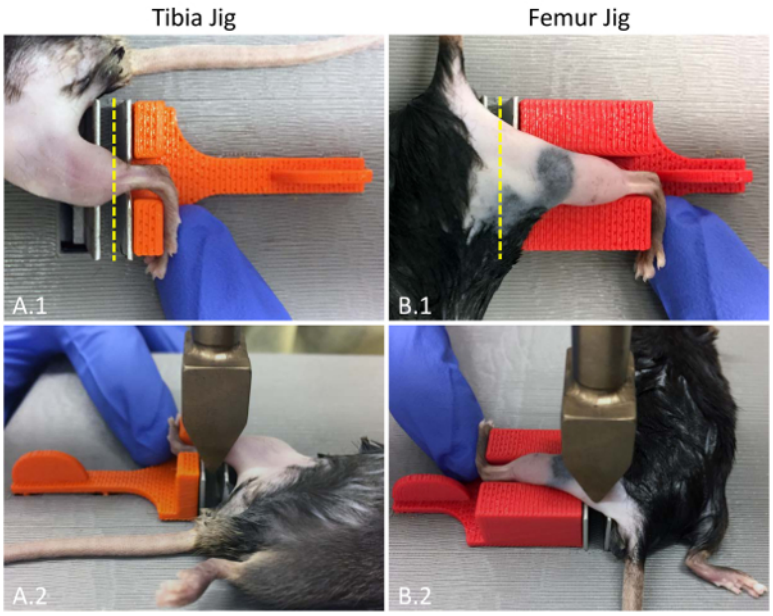

Figure 4: Tibia- and femur-fracture positioning. These are top-down photographs of (**A**) a mouse tibia**and (B**) femur in the positing jig. (**A.1**) For tibia fractures, the mouse is placed in a supine position with the tibia in the center of the support anvils and the dorsum of the foot pressed against the jig. (**B.1**) For femur fractures, the mouse is placed in a prone position with the dorsum of the foot pressed against the jig. The dashed yellow line indicates the location of the anvil impact. (**A.2** and **B.2**) The bottom photographs demonstrate the anvil location at the time of impact. The positioning of the researcher's hands should not interfere with the ram actuation. Please click here to view a larger version of this figure.

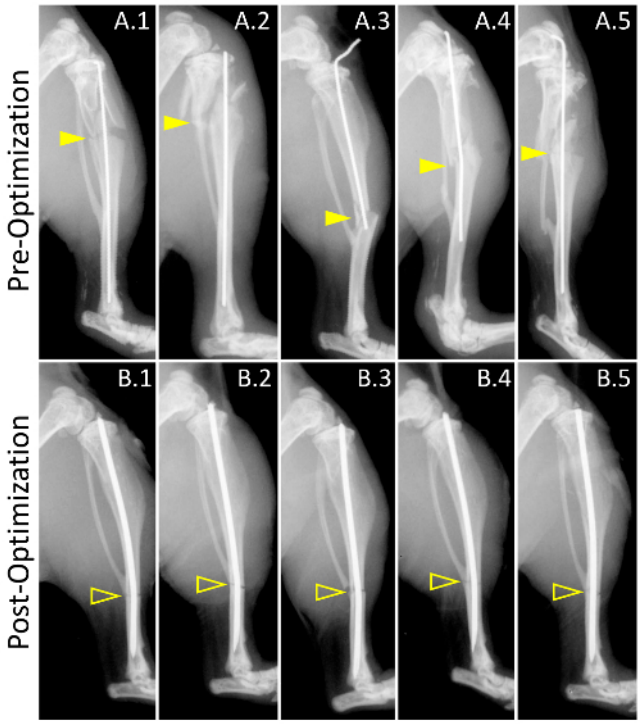

Figure 5. Pre- and post-optimization of the fracture generation. These panels show lateral radiographs of representative fractures from (**A**) pre-optimization and (**B**) post-optimization fracture groups. The size of the group was 58 mice. Solid arrowheads and arrowhead outlines indicate the level of fracture in the pre- and post-optimization groups, respectively. (**A.1** - **A.5**) The fractures generated pre-optimization demonstrate a high degree of comminution and fracture-level variability. The pin diameter only partially fills the intramedullary canal with a high degree of length variability. The pin length inconsistency resulted in (**A.3**) non-stabilized fractures and (**A.3 - A.5**) pin exposure. A lack of fracture depth control resulted in (**A.4**) bent pins and contributed to (**A.1** - **A.5**) comminution. In fractures generated post-optimization (see **Table 1** for the full set of parameters), the use of a positioning jig (**Figure 3A**) resulted in a low variability of fracture locations (yellow arrowhead outlines). The optimization of the pin width based on pre-fracture radiographs resulted in a pin selection that filled the intramedullary canal. The use of a pin cutting gauge (**Figure 3B**) resulted in a consistent pin length. The optimization of the drop height and the impact depth produced simple transverse fractures with no comminution or bent pins. Please click here to view a larger version of this figure.

		Abbreviation	Tibia	Femur
Pre-fracture parameters				
	Anvil Width (cm)	*AW*	0.40	0.40
	Ram Weight (g)	*RW*	272.00	272.00
Pre-fracture measurements				
	Limb Length (cm), mean ±SD	LL	1.75±0.03	1.32±0.05
	Cortical Diameter (cm), mean±SD	*CD*	0.10±0.00	0.15±0.01
	Medullary Diameter (cm), mean±SD	*MD*	0.05±0.00	0.09±0.01
	Pin Size (gauge/cm)	*PS*	27/3.175	23/3.810
	Center of Guillotine Impact (cm) = *AW* / 2	*CGI*	0.20	0.2
	Fracture Length (cm), mean ±SD	*FL*	0.56±0.02	0.64±0.01
Optimization				
	Pin Length (cm) = 0.9 * *LL*	*PL*	1.58	1.19
	Impact Depth (cm) = 0.75 * *CD*	*ID*	0.07	0.11
	Cutting Gauge Length (cm) = *PS* - *PL*	*CGL*	1.60	2.62
	Jig Depth (cm) = *FL* - *CGI*	*JD*	0.36	0.44
	Drop Height (cm)	*DH*	2.20	4.40
Post-fracture measurements				
	Experimental Pin Length (cm), mean±SD	*EPL*	1.60±0.06	1.19±0.04
	Experimental Pin Length to Pin Length (%)		101.1%	100.0%
	Experimental Fracture Length (cm), mean±SD	*EFL*	0.54±0.01	0.62±0.06
	Experimental Fracture Length to Fracture Length (%)		97.6%	97.1%
	Simple Transverse Fracture (%)		9/9 (100%)	9/9 (100%)

Table 1: Parameters of the fracture generation before and after the development of the new guillotine system.

	Pre-Optimization	Post-Optimization	Test	Significance
Experimental Fracture Length (cm), mean±SD	0.74±0.28	0.52±0.05	*t*	<0.001
			F	<0.001
Experimental Pin Length (cm), mean±SD	1.47±0.21	1.57±0.09	*t*	<0.001
			F	<0.001
Pin to Bone Length (%), mean±SD	83.67±11.97	92.43±5.29	*t*	<0.001
			F	<0.001
Simple Transverse Fracture (%)	46.55	98.28	*Pearson*	<0.001

Table 2: Fracture results before and after the parameter optimization.

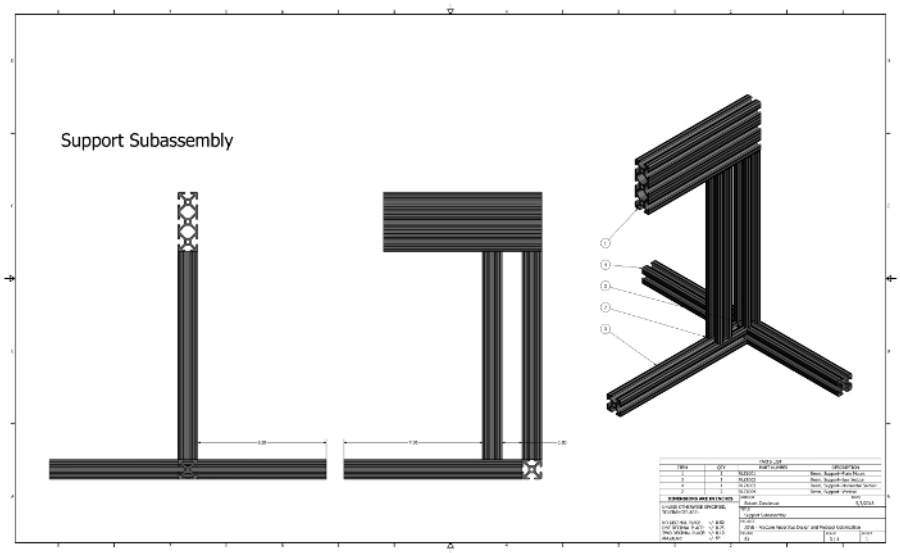

Supplementary Figure 1: Support Subassembly technical drawing. This figure shows a technical drawing for the assembly of the support components. Please click here to view a larger version of this figure.

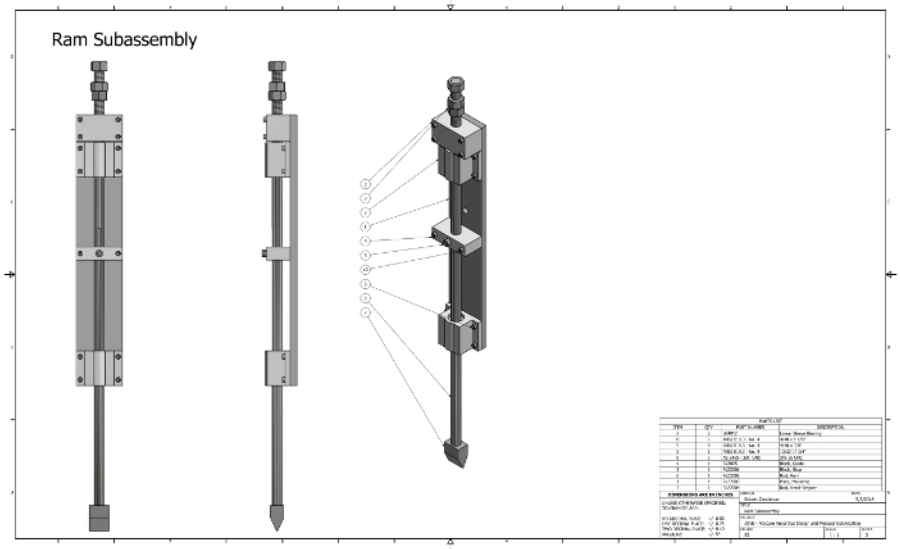

Supplementary Figure 2: Ram Subassembly technical drawing. This figure shows a technical drawing for the assembly of the ram components. Please click here to view a larger version of this figure.

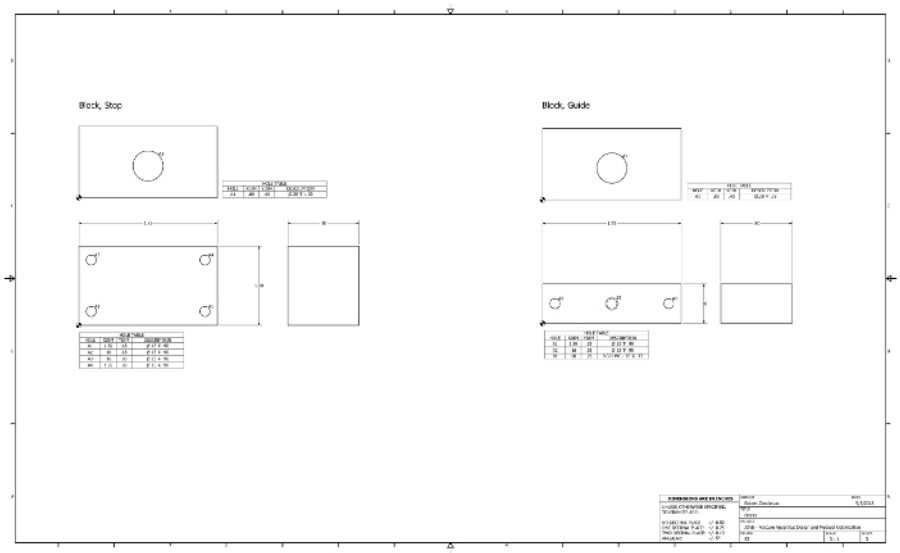

Supplementary Figure 3: Blocks technical drawing. This figure shows a technical drawing which can be used to manufacture the stop and guide blocks for the fracture apparatus. We used aluminum. Please click here to view a larger version of this figure.

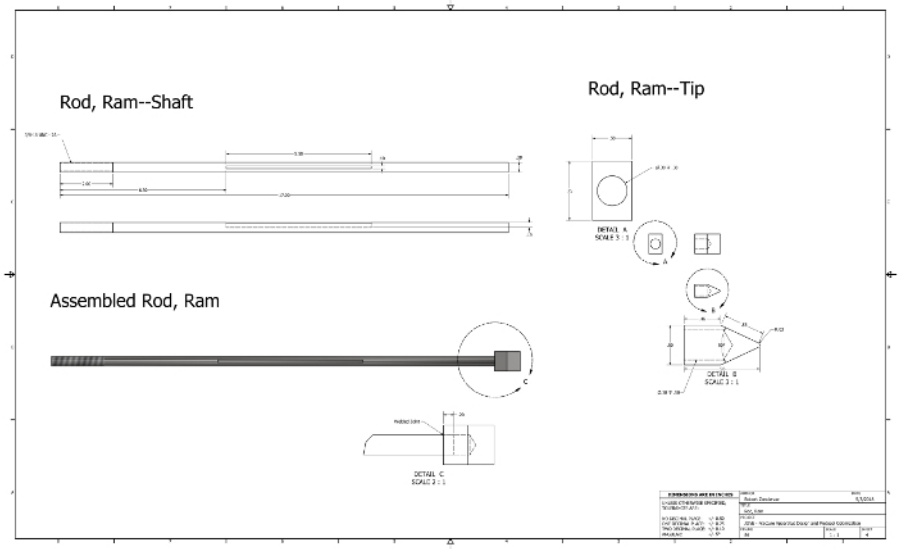

Supplementary Figure 4: Rod, Ram technical drawing. This figure shows a technical drawing which can be used to manufacture the ram for the fracture apparatus. We used stainless steel. Please click here to view a larger version of this figure.

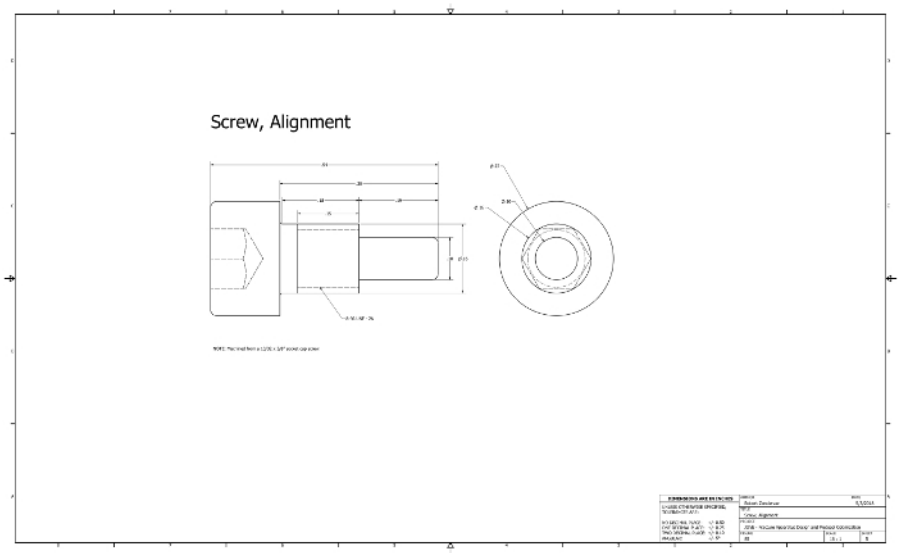

Supplementary Figure 5: Screw, Alignment technical drawing. This figure shows a technical drawing which can be used to modify a socket cap screw to align the ram. Please click here to view a larger version of this figure.

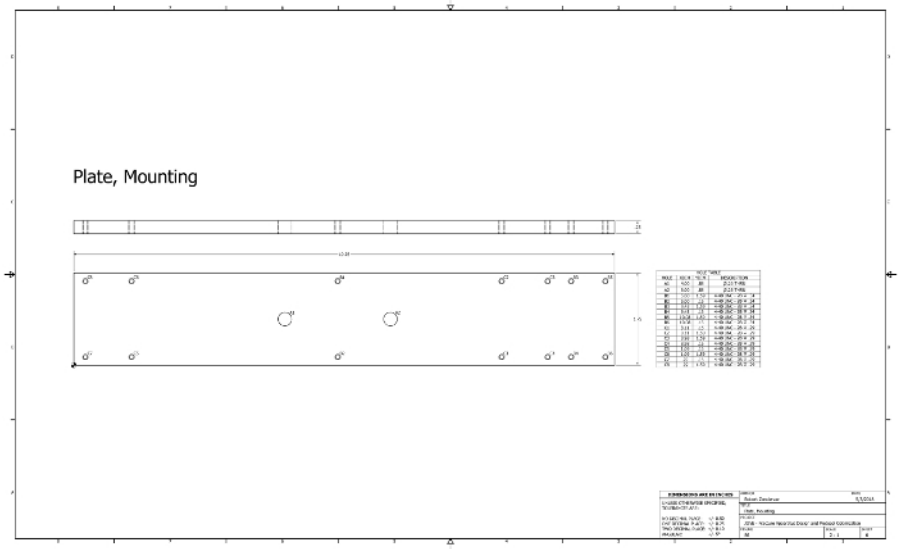

Supplementary Figure 6: Pate, Mounting technical drawing. This figure shows a technical drawing to manufacture the mounting plate for the fracture apparatus. We used aluminum. Please click here to view a larger version of this figure.

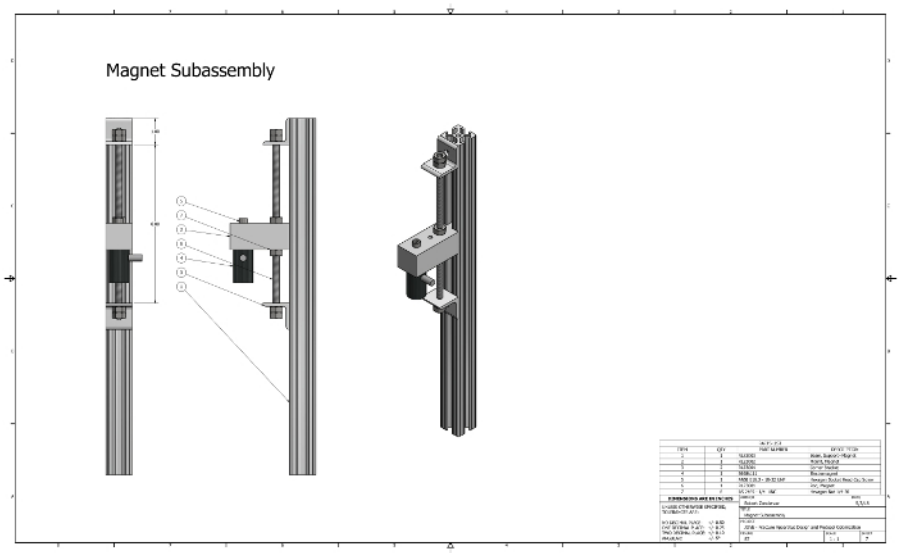

Supplementary Figure 7: Magnet Subassembly technical drawing. This figure shows a technical drawing for the assembly of the magnet components. Please click here to view a larger version of this figure.

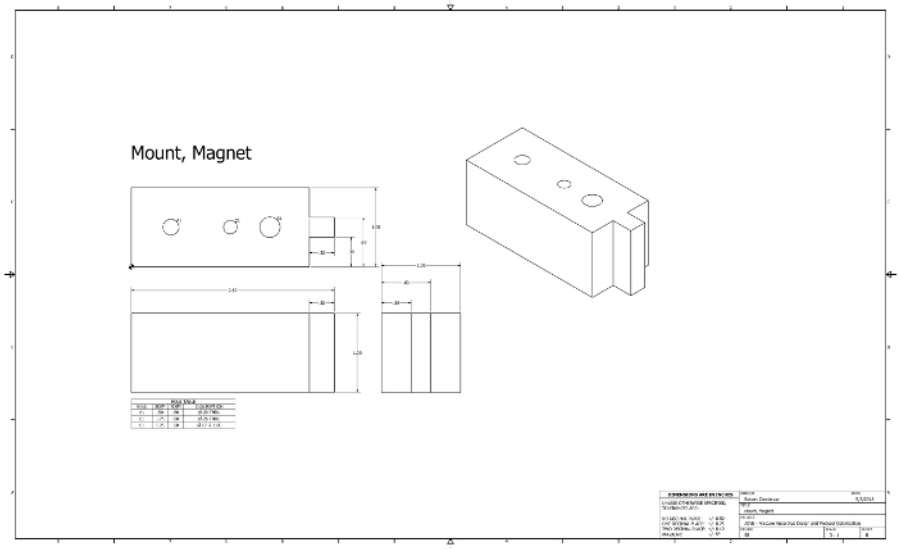

Supplementary Figure 8: Mount, Magnet technical drawing and CAD file. This figure shows (**A**) a technical drawing and (**B**) CAD file which can be used to manufacture the magnet mount (file format: *.stl). We 3D-printed the part using polylactic acid (PLA). Please click here to view a larger version of this figure.

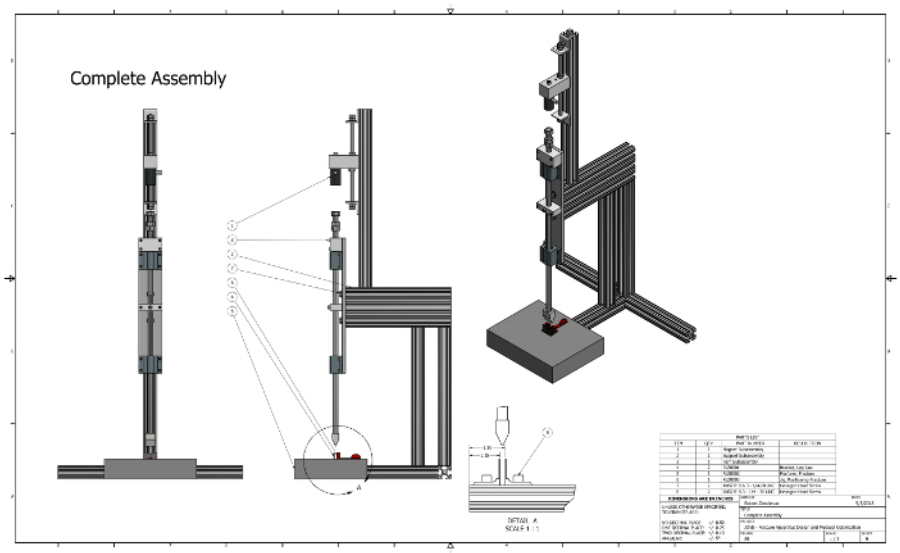

Supplementary Figure 9: Complete Assembly technical drawing and CAD file. This figure shows (**A**) a technical drawing of the complete fracture assembly with its components and (**B**) the CAD file (file format: *.iam). Please click here to view a larger version of this figure.

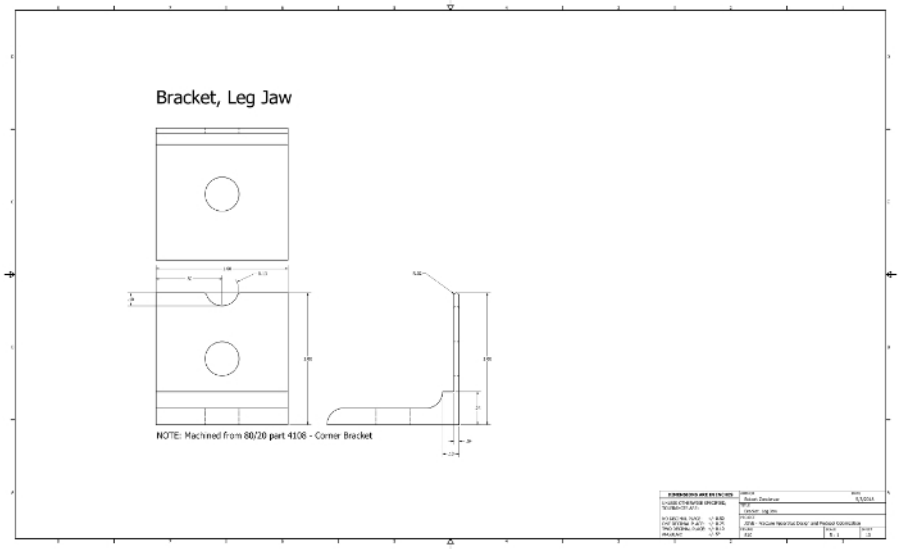

Supplementary Figure 10: Bracket, Leg Jaw technical drawing. This figure shows a technical drawing which can be used to manufacture the leg brackets for the fracture apparatus. The brackets are machined from off-the-shelf 8020 corner brackets. Please click here to view a larger version of this figure.

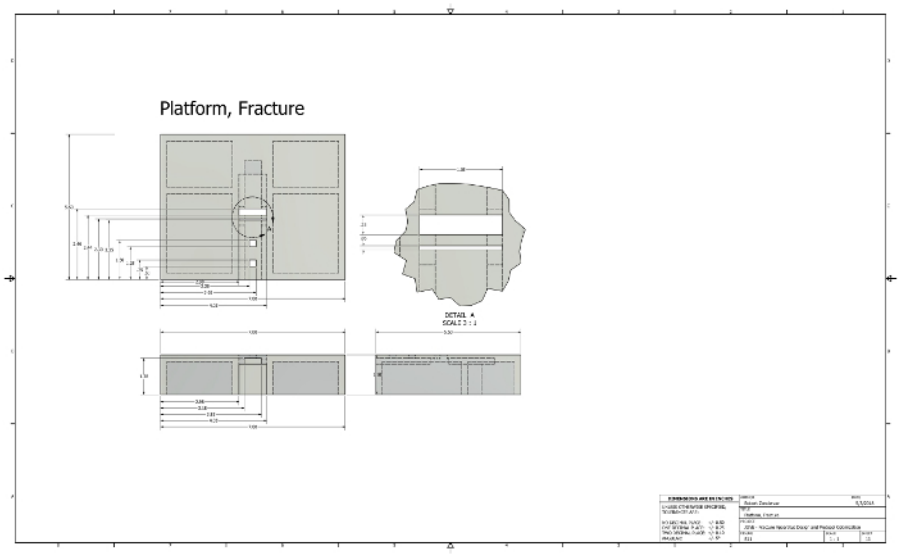

Supplementary Figure 11: Platform, Fracture technical drawing and CAD file. This figure shows (**A**) a technical drawing and (**B**) CAD file which can be used to manufacture the fracture platform (file format: *.stl). We 3D-printed the part using polylactic acid (PLA). Please click here to view a larger version of this figure.

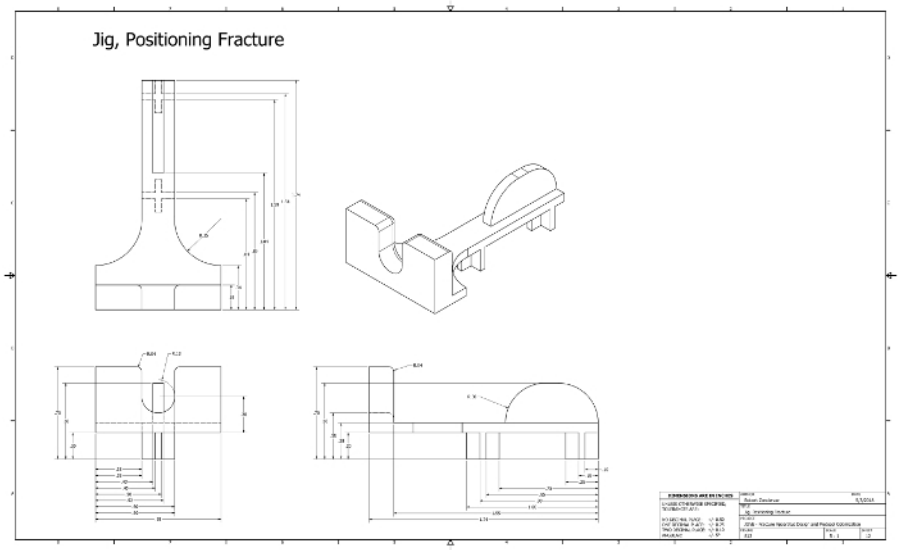

Supplementary Figure 12: Jig, Positioning Fracture technical drawing and CAD file. This figure shows (**A**) a technical drawing and (**B**) CAD file which can be used to manufacture the limb-positioning jig (file format: *.stl). We 3D-printed the part using polylactic acid (PLA). Please click here to view a larger version of this figure.

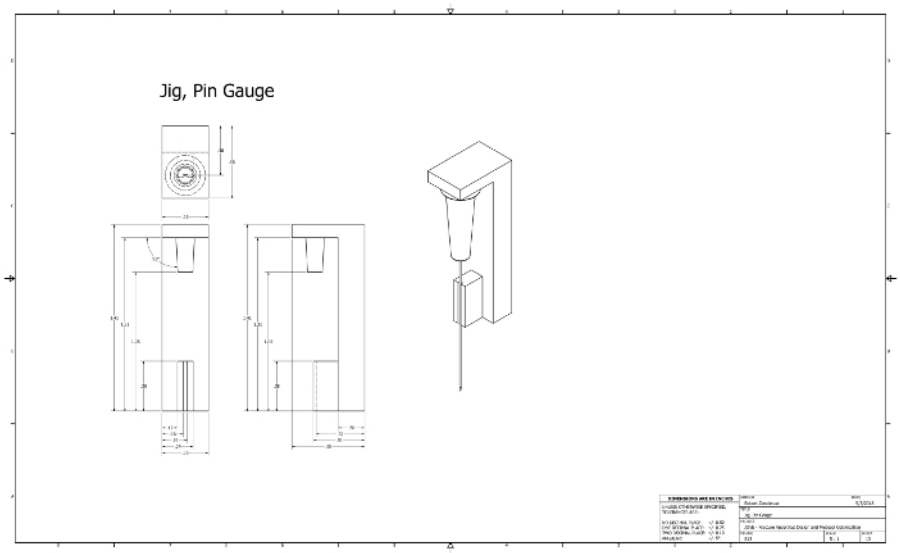

Supplementary Figure 13: Jig, Pin Gauge technical drawing and CAD file. This figure shows (**A**) a technical drawing and (**B**) CAD file which can be used to manufacture a pin cutting gauge (file format: *.stl). We 3D-printed the part using polylactic acid (PLA). Please click here to view a larger version of this figure.

Discussion

This fracture optimization and generation protocol provides researchers with an efficient method to derive at fracture parameters and perform a minimally invasive procedure, which produces precise, repeatable, transverse fractures. Additionally, this protocol establishes a common set of fracture generation parameters, which promotes method consistency amongst researchers. These parameters will enable the creation of a common fracture database to establish fracture standards based on a variety of parameters (*e.g.*, age, sex, gender, and genotype). An optimization of fracture variables significantly decreases sample heterogeneity - reducing the amount of wasted time, lost resources, and unusable data.

To generate accurate and precise fractures, it is vital to establish a standardized set of fracture generation parameters that will produce a high degree of specificity and reduce the variability of fracture locations. In addition to fracture generation, adequate stabilization is also required to promote fracture callus formation and to lessen the probability of non-union. Intramedullary pinning is a common fixation method used to stabilize appendicular long bone fractures both experimentally and clinically. Internally fixated fractures tend to heal indirectly - a process involving tissue differentiation, bone resorption at the fracture surface, and the subsequent fracture union *via* callus formation and remodeling. These processes can be impeded by movement at the fracture junction and migration of the pin within the medullary cavity. This protocol utilizes a fixation method that reduces the degree of displacement at the fracture site following fixation and limits the extent of pin migration without the use of sophisticated surgical equipment and techniques that can cause unnecessary damage to cortical bone tissue. Generating a set of pin parameters that maximize the intramedullary contact per a specific sample type provides the necessary stability for proper callus formation and bone remodeling.

Once the intramedullary pin has been placed, the next critical step is generating a simple transverse fracture. Protocols that generate fractures *via* externally applied, blunt-force trauma have the potential to produce comminuted fractures and damage fixation hardware. To mitigate these complications, it is important to control the impact depth, which has to be equal to 0.5x the average cortical diameter of each sample set[23]. Fracture comminution can also result from excessive force applied during external blunt-force trauma procedures. If the impact velocity exceeds a critical threshold, the speed of the crack propagation will generate stress waves resulting in multiple fracture sites[24]. It is critical to establish a ram weight and drop height that will generate enough kinetic energy to produce a fracture, while also remaining below the impact velocity threshold for stress wave production, reducing the possibility of comminution. A high-impact velocity will cause a rapid loading of the bone, which produces excessive energy absorption before the fracture is generated[25]. Upon fracture propagation, the excessive energy absorbed during the loading is released non-linearly, which produces comminution. A lower impact velocity and slower loading of the energy has a higher probability of producing a linear fracture compared to high-impact velocities and rapid loading[26]. To minimize the incidence of comminution, this protocol uses a standard ram weight of 250 g for mice - this can be adjusted to accommodate a larger species. When working with very young animals or with those with a known bone disease (*e.g.*, osteopenia or osteosclerosis), it may be necessary to decrease the ram weight. It is important to use a consistent ram weight when adjusting the drop height so only one variable is being optimized at a time. Calculations for species-specific ideal impact velocities will produce more consistent fractures by accounting for slight variations in the size and soft tissue morphology of the specimen.

The methods described above eliminate many shortcomings of other fracture generation protocols; however, some aspects may require training to efficiently produce desired results. One possible complication of the procedure is an inaccurate pin placement, potentially causing considerable bone or soft-tissue damage. This is due primarily to the limited visibility of the approach and a lack of sufficient bilateral hand dexterity. An internal fixation without an open incision can require a fair amount of skill from the person performing the procedure. Therefore, it is important that he or she has had sufficient training - on cadavers, if necessary - to avoid excess soft-tissue damage that could cause complications throughout the healing process. Recognizing the structures specified in the protocol (the patellar ligament, tibial plateau, and

intercondylar notch of the femur) will help produce a consistent, precise pinning with minimal soft-tissue damage. However, the goal of the described study was not to present a detailed procedure for pin placement, but rather to describe methods for generating ideal fractures.

The use of the cutting gauge is highly recommended to avoid any reaming through the proximal end of the femur or distal end of the tibia. Drilling through the proximal end of the femur could cause unnecessary damage to the soft tissue or bone in the hip, causing mobility and injury complications during the healing process. Similarly, reaming through the distal end of the tibia will damage ankle structures, altering the gait mechanics, loading, and callus formation.

To increase the accuracy of the fracture location, a custom limb-positioning jig can be designed to ensure the proper positioning of the limb within the device. A precise and accurate impact placement is essential to consistently generate fractures at the desired location. Our laboratory currently employs two jigs: one for mid-tibial fractures and the other for mid-femoral fractures, but the versatility of a modular design and 3D printing gives researchers the capability to generate fractures at a variety of locations. The addition of a custom jig designed to generate fractures in a particular location increases both the accuracy and precision of fracture generation by limiting the likelihood of operator errors.

The few limitations of this method are similar to those encountered in other existing closed fracture techniques. Excessive soft tissue or fat can impede the generation of fractures, as seen in older or overweight mice. It is important to note that this is normally due to a lack of force and not to a lack of impact depth. This limitation can be overcome by increasing either the ram weight or the velocity to increase the kinetic energy applied to the fracture site. This method also relies upon internal fixation, which can disrupt the endosteal surface of the bone and affect the healing. While endosteal disruption also occurs clinically with intramedullary nailing, if the contribution of endosteum to fracture repair is being studied, external fixation or plates may be a better option. An additional limitation is the required sample of sacrificial animals to establish the initial parameters; however, as the fracture variables for more sample types are established and the database develops, the need for additional sacrificial samples should decrease.

The described protocol increases the precision of induced traumas through the use of standardized parameters specific to sample type, minimizing the fracture heterogeneity typically seen in closed fracture generation procedures. Most current fracture generation protocols are applicable to only murine species and produce moderately consistent fractures. They often require the use of a specific sample type to obtain optimal results or do not account for variations within strains. The protocol presented here accounts for variation in size or bone morphology that may exist between mouse strains and can be adapted to generate consistent fractures in other species. In addition, the widespread application of this protocol will support the adoption of a standardized fracture language between researchers. Using similar protocols with common variables will improve the method consistency and strengthen comparisons between studies. While the parameters discussed above are specific to murine long bones, there is the potential for the fracture optimization protocol to be used in additional fracture models, further increasing the versatility of a collective fracture generation parameter database. Employing this fracture optimization protocol will increase the production of homogeneous, usable samples by improving the consistency of the fracture location and pattern. The higher percent yield of the samples will decrease the waste of laboratory resources, reduce the number of animals needed, and improve study efficiency.

Disclosures

The authors have nothing to disclose.

Acknowledgements

The research reported in this publication was supported by the National Institute of Arthritis and Musculoskeletal and Skin Diseases of the National Institutes of Health under award number F30AR071201 and R01AR066028.

References

1. *BMUS: The Burden of Musculoskeletal Diseases in the United States.* http://www.boneandjointburden.org/ (2014).
2. Corso, P., Finkelstein, E., Miller, T., Fiebelkorn, I., Zaloshnja, E. Incidence and lifetime costs of injuries in the United States. *Injury Prevention.* **12** (4), 212-218 (2006).
3. Nguyen, N.D., Ahlborg, H.G., Center, J.R., Eisman, J.A., Nguyen, T.V. Residual lifetime risk of fractures in women and men. *Journal of Bone and Mineral Research: The Official Journal of the American Society for Bone and Mineral Research.* **22** (6), 781-788 (2007).
4. Thompson, Z., Miclau, T., Hu, D., Helms, J.A. A model for intramembranous ossification during fracture healing. *Journal of Orthopaedic Research: Official Publication of the Orthopaedic Research Society.* **20** (5), 1091-1098 (2002).
5. Cheung, K.M.C., Kaluarachi, K., Andrew, G., Lu, W., Chan, D., Cheah, K.S.E. An externally fixed femoral fracture model for mice. *Journal of Orthopaedic Research.* **21** (4), 685-690 (2003).
6. Connolly, C.K. *et al.* A reliable externally fixated murine femoral fracture model that accounts for variation in movement between animals. *Journal of Orthopaedic Research.* **21** (5), 843-849 (2003).
7. Histing, T. *et al.* An internal locking plate to study intramembranous bone healing in a mouse femur fracture model. *Journal of Orthopaedic Research.* **28** (3), 397-402 (2010).
8. Gröngröft, I. *et al.* Fixation compliance in a mouse osteotomy model induces two different processes of bone healing but does not lead to delayed union. *Journal of Biomechanics.* **42** (13), 2089-2096 (2009).
9. Bonnarens, F., Einhorn, T.A. Production of a standard closed fracture in laboratory animal bone. *Journal of Orthopaedic Research.* **2** (1), 97-101 (1984).
10. Huang, C. *et al.* The spatiotemporal role of COX-2 in osteogenic and chondrogenic differentiation of periosteum-derived mesenchymal progenitors in fracture repair. *PloS One.* **9** (7), e100079 (2014).
11. Waki, T. *et al.* Profiling microRNA expression during fracture healing. *BMC Musculoskeletal Disorders.* **17**, 83 (2016).
12. Yee, C.S. *et al.* Sclerostin antibody treatment improves fracture outcomes in a Type I diabetic mouse model. *Bone.* **82**, 122-134 (2016).

13. Wong, E. *et al.* A novel low-molecular-weight compound enhances ectopic bone formation and fracture repair. *The Journal of Bone and Joint Surgery. American Volume.* **95** (5), 454-461 (2013).
14. Prodinger, P.M. *et al.* Does Anticoagulant Medication Alter Fracture-Healing? A Morphological and Biomechanical Evaluation of the Possible Effects of Rivaroxaban and Enoxaparin Using a Rat Closed Fracture Model. *PloS One.* **11** (7), e0159669 (2016).
15. Menzdorf, L. *et al.* Local pamidronate influences fracture healing in a rodent femur fracture model: an experimental study. *BMC Musculoskeletal Disorders.* **17**, 255 (2016).
16. Hagiwara, Y. *et al.* Fixation stability dictates the differentiation pathway of periosteal progenitor cells in fracture repair. *Journal of Orthopaedic Research: Official Publication of the Orthopaedic Research Society.* **33** (7), 948-956 (2015).
17. Gardner, M.J. *et al.* Differential fracture healing resulting from fixation stiffness variability: a mouse model. *Journal of Orthopaedic Science: Official Journal of the Japanese Orthopaedic Association.* **16** (3), 298-303 (2011).
18. Catma, M.F., *et al.* Remote ischemic preconditioning enhances fracture healing. *Journal of Orthopaedics.* **12** (4), 168-173 (2015).
19. Lichte, P. *et al.* Impaired Fracture Healing after Hemorrhagic Shock. *Mediators of Inflammation.* **2015**, 132451 (2015).
20. Lopas, L.A. *et al.* Fractures in geriatric mice show decreased callus expansion and bone volume. *Clinical Orthopaedics and Related Research.* **472** (11), 3523-3532 (2014).
21. Bonnarens, F., Einhorn, T.A. Production of a standard closed fracture in laboratory animal bone. *Journal of orthopaedic research.* **2** (1), 97-101 (1984).
22. Marturano, J.E. *et al.* An improved murine femur fracture device for bone healing studies. *Journal of Biomechanics.* **41** (6), 1222-1228 (2008).
23. Jackson, R.W., Reed, C.A., Israel, J.A., Abou-Keer, F.K., Garside, H. Production of a standard experimental fracture. *Canadian Journal of Surgery. Journal Canadien De Chirurgie.* **13** (4), 415-420 (1970).
24. Byrne, M., Cleveland, B., Marturano, J., Wixted, J., Billiar, K. Design of a reproducible murine femoral fracture device. Conference: Bioengineering Conference, 2007. *NEBC '07. IEEE 33rd Annual Northeast.* (2007).
25. Carter, D.R., Hayes, W.C. Compact bone fatigue damage-I. Residual strength and stiffness. *Journal of Biomechanics.* **10** (5), 325-337 (1977).
26. McGee, A., Qureshi, A., Porter, K. Review of the biomechanics and patterns of limb fractures. *Trauma.* **6** (1), 29-40 (2004).

